On the Growth of Al_2O_3 Scales

A.H. Heuer[1,4,*], T. Nakagawa[1], M.Z. Azar[1], D.B. Hovis[1], J.L. Smialek[2], B. Gleeson[3], N.D.M. Hine[4,5], H. Guhl[4,6], H-S. Lee[4,6] P. Tangney [4,6], W.M.C. Foulkes[6], and M.W. Finnis[4,6]

Abstract

Understanding the growth of Al_2O_3 scales requires knowledge of the details of the chemical reactions at the scale/gas and scale/metal interfaces, which in turn requires specifying how the creation/annihilation of oxygen and Al vacancies occurs at these interfaces. The availability of the necessary electrons and holes to allow for such creation/annihilation is a crucial aspect of the scaling reaction. The electronic band structure of polycrystalline Al_2O_3 thus plays a decisive role in scale formation and is considered in detail, including the implications of a DFT calculation of the band structure of a $\Sigma 7$ $\{4\ \bar{5}\ 10\}$ bicrystal boundary, for which the atomic structure of the boundary was known from an independent DFT energy minimization calculation and comparisons with an atomic resolution transmission electron micrograph of the same boundary. DFT calculations of the formation energy of oxygen and Al vacancies in bulk Al_2O_3 in various charge states as a function of the Fermi energy suggested that electronic conduction in Al_2O_3 scales most likely involves excitation of both electrons and holes, which are localized on singly charged oxygen vacancies, $V_O^{\bullet}$ and doubly charged Al vacancies, V_{Al}'', respectively. We also consider the variation of the Fermi level across the scale and bending ("tilting") of the conduction band minimum and valence band maximum due to the electric field developed during the scaling reaction. The band structure calculations suggest a new mechanism for the "reactive element" effect – a consequence of segregation of Y, Hf, etc. to grain boundaries in Al_2O_3 scales, which results in improved oxidation resistance; namely, that the effect is due to the modification of the near-band edge grain-boundary defect states rather than any blocking of diffusion pathways, as previously postulated.

Secondly, Al_2O_3 scale formation is dominated by grain boundary as opposed to lattice diffusion, and there is unambiguous evidence for both oxygen and Al countercurrent transport in Al_2O_3 scale-forming alloys. We postulate that such transport is mediated by migration of grain boundary disconnections containing charged jogs, rather than by jumping of isolated point defects in random high angle grain boundaries.

[1] Department of Materials Science and Engineering, Case Western Reserve University, Cleveland, Ohio 44106
[2] NASA Glenn Research Center, Cleveland, Ohio 44135
[3] Department of Mechanical Engineering and Materials Science, University of Pittsburgh, Pittsburgh, PA 15261
[4] Department of Materials, Imperial College, London, England SW7 2AZ
[5]Cavendish Laboratory, University of Cambridge, England CB3 0HE
[6]Department of Physics, Imperial College London, England SW7 2AZ

This work relates to Department of the Navy Grant N62909-12-1-7124 issued by the Office of Naval Research Global.

I. Introduction

Ni-base and Fe-base structural alloys exposed to the highest operating temperatures (i.e. > 900°C) in oxidizing ambients invariably depend on formation of a passivating Al_2O_3 scale for the requisite oxidation resistance, and a sizeable literature on Al_2O_3 scale formation is available [1-7]. The protection afforded by the Al_2O_3 scales arises from the sluggish diffusion kinetics of both oxygen and Al [8]; lattice diffusion is so slow that scale formation kinetics are dominated by grain-boundary diffusion. Furthermore, there is good evidence from alloys such as NiCrAls and FeCrAls that scale formation involves dominant inward oxygen diffusion, combined with significant outward aluminum diffusion, the diffusion pathways being on grain boundaries [9, 10].

We recently suggested [11] that an important aspect of this complex electrochemical phase transformation, the availability of electrons (e') and holes ($h^{\bullet}$) for Al and oxygen vacancy formation and annihilation at both the scale/gas and scale/metal interfaces, necessitates consideration of the electronic (band) structure of polycrystalline Al_2O_3. This had not been sufficiently considered in the prior literature on Al_2O_3 scale formation, and we noted that segregation of "reactive elements" (REs) such as Y, Zr, Hf, etc. from the alloy substrate to oxide grain boundaries in scales formed on NiCrAlYs and FeCrAlYs could modify the density of near-band edge grain boundary donor and acceptor states [11]. In this view, production/annihilation of cation vacancies at the scale/gas and scale/metal interfaces via the reactions

$$3O_2 + 12e' \rightarrow 4V_{Al}''' + 6O_O^x \qquad (1)$$

and

$$Al_M + V_{Al}''' \rightarrow Al_{Al}^x + V_M + 3e' \quad (2)$$

may be impeded by the lack of availability of the electrons that are an essential part of eqns. 1 and 2. A dearth of electronic charge carriers to allow eqns. (1) and (2) to proceed could cause reduction in δD_{gb}^{Al} (D_{gb}^{Al} the Al grain boundary diffusivity, δ the grain boundary width) and thus account for the observed decrease in the rate of Al_2O_3 scale growth on RE-containing alloys [7]. (Here, Kröger-Vink notation is used, and Al_M and V_M without superscripts in eqn. 2 represent an Al atom and metal vacancy in the Al_2O_3 scale-forming alloy. We furthermore ignore the possibility of diffusion of Al or oxygen interstitials, $Al_i^{\bullet\bullet\bullet}$ and O_i'', contributing to mass transport during the scaling reaction, and focus on the majority vacancy point defects. This is justified by the high energy of these interstitial point defects relative to vacancy point defects, V_{Al}''' and $V_O^{\bullet\bullet}$, as can be seen in Fig.9 of ref. [11]. Of course, the high energies of those interstitials result in low interstitial point defect concentrations).

The best-known alternative explanation of the RE effect involves "site blocking" [6], the notion that the segregation of REs to scale grain boundaries impedes outward Al grain boundary diffusion via a steric effect. This alternative explanation involves the near-universal assumption that enhanced grain-boundary diffusion involves point defect jumping in the relatively open structure of random high-angle grain boundaries, a notion which we question in this paper.

Our focus on the band structure of Al_2O_3 scales was motivated by recent work [12-15] measuring the oxygen permeability in dense Al_2O_3 ceramics subject to pO_2 gradients at elevated temperatures. For those experiments, eqn. (1) at the high pO_2 interface and the corresponding oxygen vacancy reaction at the low pO_2 interface

$$2O_O^x \rightarrow 2V_O^{\bullet\bullet} + O_2 + 4e' \quad (3)$$

were invoked to explain the oxygen pressure dependence of the oxygen permeability data [12].

These permeability data have direct relevance to scale growth, as large pO_2 gradients are present across growing scales; the permeability data can be used to extract δD_{gb}^{O} (oxygen grain boundary diffusivities) at low oxygen pressures, and δD_{gb}^{Al} at high oxygen pressures, and revealed that Al_2O_3 exhibited *n*-type *ionic* behavior at low oxygen pressures -- δD_{gb}^{O} varying as $(pO_2)^{-1/6}$ -- and *p*-type *ionic* behavior at high oxygen pressures -- δD_{gb}^{Al} varying as $(pO_2)^{+3/16}$. These observed pressure dependencies follow directly from the defect reactions (1) and (3) above [12].

The implications for scale formation are that there may be a *p*-*n* ionic transition somewhere in the scale (we treat *p*-type and *n*-type *electronic* behavior in Section II). The *p*-*n* boundary occurs close to the scale/gas interface, for the usual case of oxidation in air, whereas *n*-type behavior could prevail throughout the scale if oxidation occurs at a sufficiently low oxygen pressure.

Figure 1 schematically shows the expected variation in oxygen chemical potential (μ_o) as a function of position within a growing scale. This figure agrees with previous studies on the variation in oxygen chemical potential within a scale [15,16], but differs from that proposed by Young *et al.* [17], who suggested that μ_O remains relatively high through most of the scale thickness. This view cannot be rationalized with kinetic results pertaining to Al_2O_3 scale growth as a function of $p(O_2)$ (e.g. ref. [18]). On a related note and owing to a lack of relevant data until very recently, it has invariably been assumed

that for scale growth, both δD_{gb}^{O} and δD_{gb}^{Al} are independent of oxygen pressure and constant across the scale. However, the oxygen pressure dependence revealed by the permeability experiments has allowed us to satisfactorily compare the activation energies derived from grain-size dependent parabolic rate constants and activation energies derived from so-called double oxidation experiments (oxidation first in $^{16}O_2$ and then in $^{18}O_2$); this will be described elsewhere [19]. One final comment: neither the electrical properties of Al_2O_3 scales nor the possibilities of oxygen pressure-dependent diffusivities have figured prominently in the recent literature on Al_2O_3 scale formation [1-7].

The growth of Al_2O_3 scales differs from growth of other oxide scales such as NiO on Ni and SiO_2 on Si; transition metal oxides such as NiO usually form by outward lattice diffusion of cations, while SiO_2 forms by inward diffusion of oxygen molecules through the amorphous oxide. For Al_2O_3 scales, in addition to scaling kinetics being dominated by grain-boundary diffusion and perceived impurity effects, the so-called transition aluminas (cubic or near-cubic Al_2O_3 polymorphs with defect spinel structures) are usually the first oxidation products; they subsequently transform to the stable and denser corundum (α) polymorph.

In this paper, we discuss growth of Al_2O_3 scales in the framework of Wagner's classic oxidation theory [20] (Section II), recognizing that t_i, the transference number (the ratio of ionic conductivity, σ_i, to the total conductivity, which is the sum of σ_i and σ_e, the electronic conductivity), is of the order 0.5 and not $<<1$, as it is for NiO and other transition metal oxides. Section III will discuss the importance of line defects to Al_2O_3 scale formation.

II. Wagnerian Oxidation

Wagner, in his classic theory on metal oxidation [20], emphasized the need for both mass and charge transport across a growing oxide scale. There have been many reviews of Wagner's theory in the intervening years and the following points are now clear.

Scale growth kinetics will be determined by the faster diffusing ionic species, metal or oxygen, assuming electronic transport is not rate-controlling. Whichever species dominates, electronic and ionic transport must occur, with the electrons or holes being necessary to ionize metal and oxygen atoms at the scale/gas and scale/metal interfaces. If outward Al transport dominates (inward diffusion of Al vacancies), new oxide will appear at the scale/gas interface and will be described by eqn. (1), while consumption of metal atoms at the scale/metal interface will be described by eqn. (2). In other words, cation vacancies are annihilated at the scale/metal interface, equivalent to recession of the metal (displacement of the scale/metal interface), with new oxide lattice sites being created (the right hand side of eqn. (1)). Further, as metal vacancies are injected into the alloy substrate (eqn. (2)), suitable vacancy sinks in the substrate must be available. There is extensive evidence in the literature to show that vacancies formed by a selective oxidation process can both be annihilated at the oxide-metal interface [21,22] and can be injected into the underlying metal [23-26].

For scale growth by inward oxygen diffusion, oxygen vacancies must be annihilated at the scale/gas interface by a reaction of the form

$$O_2 + 2V_O^{\bullet\bullet} \rightarrow 2O_O^x + 4h^{\bullet} \qquad (4)$$

with growth of new oxide and consumption of substrate metal occurring at the scale/metal interface.

$$2Al_M \rightarrow 3V_O^{\bullet\bullet} + 2Al_{Al}^{x} + 2V_M + 6e' \tag{5}$$

Similar to the cation transport case, there must be a sink in the metal for annihilation of the metal vacancies created by eqn. (5).

We further consider transport issues and vacancy production/annihilation in Section III. Here, we are concerned with the availability of the electrons and holes required to sustain the scaling reaction. Inasmuch as the diffusing species are electrically charged and have different mobilities, electric fields will develop during scaling. If the voltage developed across an oxide scale is probed using chemically inert electrodes such as Pt, then the electrical potential, V, at the scale/gas interface (relative to the metal) developed by the electrochemical potential across the scale will be given by:

$$V = -\frac{\Delta G_{Al_2O_3}}{6|e|}\bar{t}_i \tag{6}$$

where $\Delta G_{Al_2O_3}$ is the free energy of formation of Al_2O_3, e is the electronic charge, and $\bar{t}_i$ is a weighted mean transference number across the scale [27]. It can also be shown that if new oxide is created at the interfaces, and if the electrical current has zero divergence, new oxide will be created at a rate

$$J = \frac{\sigma}{12} t_i t_e \nabla \mu_o \text{ formula units per unit area per second,} \tag{7}$$

where $t_e = 1 - t_i$ and $\nabla \mu_o$ is the gradient in the oxygen chemical potential. Both σ and t_i can vary through the scale thickness.

Transition metal oxides typically have very low values of t_i, whereas the ionic and electronic conductivities of Al_2O_3 are similar, and appear to be a function of position within the scale (essentially a function of μ_o [16,19]). Equation (7) makes no assumptions about the ions responsible for transport, but it requires local equilibrium of oxygen, aluminum and their ions at each point on the path through the scale.

Figure 2 shows a schematic density of states diagram for polycrystalline Al_2O_3. There is a significant number of grain-boundary states extending into the gap region from both the oxygen 2p antibonding valence band and the hybridized Al 3s/3p conduction band. The room-temperature single crystal band gap is known from optical studies to be 8.8 eV[28]; it is doubtful if such a large band gap could play any role in the scaling reaction. On the other hand, oxygen and Al vacancies, with their formal charges of +2 and -3, respectively, occupy relatively deep levels in the band gap, and we suggest that they play a crucial role in scale formation, due to their proximity to the grain-boundary donor and acceptor levels shown in the figure; these are thermodynamic transition levels calculated from total energies. The Fermi level, ε_F, the chemical potential of the electrons, is somewhere in the middle of the band gap.

Figure 3 shows the projected electron densities of states (DOS) in a Σ7 symmetric boundary with a $\{4\bar{5}10\}$ boundary plane computed within density functional theory (DFT) using the GGA-PBE functional for the exchange-correlation and ultra-soft pseudo-potentials as implemented in the CASTEP code [29]. With a plane wave basis set of the size corresponding to a cut-off energy of 600 eV and an even Monkhorst-Pack grid with at least one k-point per 0.25 $\AA^{-3}$ for the sampling of the Brillouin zone, we ensured that

the numerical errors of the electronic eigenvalues are sufficiently small not to affect the conclusions in any way.

Figure 3(a) refers to a pristine dopant-free boundary, while Fig. 3(b) illustrates the effect on the DOS of replacing on Al atom in the boundary core region with a Y atom. The precise details of these computations will be published elsewhere; however, it should be noted that after minimizing the grain boundary energy, the atomic coordinates essentially reproduced the transmission electron micrograph of such a boundary shown in ref. [30]. The upper panels in Fig. 3(a) and Fig. 3(b) show the respective total DOS, whereas the other panels highlight the individual contributions of the oxygen and aluminum atoms within the grain boundary core region (the two topmost panels, marked "Oxygen GB", "Aluminium (GB)") as well as the bulk-like region of the grains (the two lowest panels).

In the pristine boundary (Fig. 3(a)), the occupied states on the oxygen atoms in the grain boundary clearly peak prominently at about ~0.5 eV above the valence band maximum, whereas empty states appear well below the conduction band minimum, which are localized at the Al ions in the same region. As can be seen in Fig. 3(b), doping the crystal with Y has substantial effects on the occupied grain boundary states, as their population is significantly diminished (*cf*. Fig 3(a), second panel). This in turn has profound implications for the creation of Al vacancies at the scale/gas interface (eqn. 1) and for the ionic and electronic conductivities. Such an effect was postulated in our recent "New Perspective" paper [11] as a possible explanation for the RE effect.

As noted above, the ionic and electronic conductivities of Al_2O_3 scales are comparable. To assess the development of electrical fields during the scaling reaction, it

is convenient to discuss the limiting conditions of $\sigma_i > \sigma_e$ or $\sigma_e > \sigma_i$, as is shown in Fig. 4. (For simplicity, we neglect the non-linearity of the electrochemical potential across the scale.) In all cases, we need to consider separately formation of new oxide at the scale/metal interface (inward oxygen ion diffusion, outward oxygen vacancy diffusion, Figs. 4a and 4c) and new oxide formation at the scale/gas interface (outward Al ion diffusion, inward Al vacancy diffusion, Figs. 4b and 4d). The usual assumption of diffusion-controlled oxidation implies local thermodynamic equilibrium (at least approximately) and establishes the position of the Fermi level relative to the energy of the defect states (see Fig. 5 below).

Consider Fig. 4a first. Here, ionic transport is faster than electronic transport, and new oxide is forming at the scale/metal interface. The Fermi level, ε_F, is pinned at the scale/metal interface by its value in the metal, which also pins the $V_O^{\bullet\bullet}/V_O^{\bullet}$ level (ε^{Vo}) shown in Fig. 2, and varies approximately linearly with position across the scale, i.e. with the variation in μ_0 , the oxygen chemical potential. The Fermi level is pinned at the scale/ gas interface by $\varepsilon^{V_{Al}}$, the energy of the V_{Al}'''/V_{Al}'' defect state shown in Fig. 2. Excess negative charge builds up on the scale/metal interface, i.e., the electric field that develops is pointing inwards. This field causes band bending (actually band "tilting") of ε_{CBM}, the conduction band minimum, ε_{VBM}, the valence band maximum, $\varepsilon^{V_{Al}}$, and ε^{V_O}, the energy of the $V_O^{\bullet\bullet}/V_O^{\bullet}$defect state.

The positions of the Fermi level at the two interfaces are important, as these interfaces are where ionization of oxygen and Al atoms can occur, as described by eqns. 1, 2, 4, and 5. (The band diagram representations presented in these figures are analogous to those used many years ago by Hauffe and Morrison [31] to assess space-

charge effects on scale-growth kinetics.) The band tilting for the valence band maximum, ε_{VBM}, and conduction band minimum, ε_{CBM}, can be significant, as voltages >1V have been measured across growing Al_2O_3 scales [32]. The specific variation of ε_F with position across the scale in Figs. 4a and 4b is considered below, in the context of discussing the nature of electron and hole transport within the scale.

We further note that transport is occurring under the driving force of both the electric field and the chemical potential gradient established by the reaction

$$3O_2 + 4Al_M \rightarrow 4Al_{Al}^x + 6O_O^x \quad (8)$$

and that when ionic conductivity is greater than the electronic conductivity, as in Figs. 4a and 4b, the charged oxygen vacancies and holes are diffusing ***against*** the electric field. Lastly, the voltage given by eqn. (6) is the difference in the electrochemical potential, the combination of band tilting and the chemical potential of the electrons defined with respect to the band edges; it is always negative, whatever the sign of the electric field.

Figure 4b is essentially identical, except for the chemical reactions at the scale/gas and scale/metal interfaces; in this case, new oxide is forming at the external interface.

The situation for the case where $\sigma_e > \sigma_i$ is very different (Figs. 4c and 4d). The electric field is pointing outward, and the Fermi level shows more modest tilting across the scale; it is again pinned at the scale/metal interface by its level in the metal and at the scale/gas interface by $\varepsilon^{V_{Al}}$. Band tilting is again significant, although in the opposite sense than in Figs. 4a and 4b, because of the opposite sign of the electric field. In this case, charged Al vacancies and electrons are diffusing against the electric field.

Although it is clear [9,10] that ionic transport is restricted to scale grain boundaries, whether electron/hole transport occurs in the bulk or preferentially along

grain boundaries is still an open question. Whichever transport path dominates, and as indicated in Fig. 4, holes will migrate towards the scale/metal interface; we conjecture that the holes are localized on Al vacancies, i.e. the Al vacancies become doubly-charged, V_{Al}''. On the other hand, electrons are conjectured to be localized at what result in singly charged oxygen vacancies, $V_O^{\bullet}$, and will migrate towards the scale/gas interface.

This picture is motivated by the results of bulk DFT calculations of the energy and charge states of point defects as a function of $p(O_2)$ and Fermi energy (Fig. 5), reproduced here from ref. [33], which utilized the local density approximation for exchange and correlation. We note that using hybrid functional calculations with the HSE06 exchange correlation functional, which would be expected to be more accurate with respect to positions of defect states within the bandgap, Choi et *al.* obtained a broadly similar qualitative picture of defect formation energies and transition levels [34]. For charged defects, the formation energy is of course dependent on the electron chemical potential, here indicated by the Fermi level with respect to the valence band maximum of the perfect crystal. The Fermi energy at 0 K can be determined self-consistently, taking into account all point defect species and charge states which have sufficiently low formation energies to be present in high concentration; these calculations will be published elsewhere. Results for a typical oxidation temperature of 1250 K are shown in Fig. 5.

For nominally pure Al_2O_3, defect equilibrium is dominated by fully ionized oxygen and Al vacancies, whose local concentrations are ultimately subject to the Schottky equilibrium product (eqn. 9).

$$[V_{Al}'''']^2[V\ddot{o}]^3 = K_S \qquad (9)$$

where the Schottky equilibrium constant, K_S, depends on the formation energies of the two kinds of vacancies, and is independent of pO_2. A self-consistent value of the Fermi energy can be determined using this equilibrium condition, locating it within the gap. While the choice of XC functional does indeed significantly influence the values of crossover points between different charge states as a function of the Fermi energy, when the Fermi level corresponding to Schottky equilibrium is determined (for each functional), the resulting formation energies agree closely between functionals, making this conclusion relatively robust. As can be seen from Figure 1 of Ref [34], Al interstitials may also be present in non-negligible quantities, in which case a more careful determination of defect species would be required, taking into account the full range of defects that might be present. In the current work, we restrict ourselves to the case of Al and O vacancies in their full charge states, as these are expected to be the majority defect species under a range of realistic conditions. Figures 5a and 5b show the formation energy of oxygen and Al vacancies as a function of the Fermi energy, ε_F, at 0.2 atm and at 10^{-31} atm (the approximate pO_2 at the scale/gas and scale/metal interfaces [19]), respectively. In these figures, the slopes of the V_{Al} and V_O lines change where the dominant charge state of these vacancies change. At the scale/gas interface (Fig. 5a), the dominant charge state for Al vacancies is -3 for Fermi energies above ~1eV, while oxygen vacancies are fully ionized at all Fermi energies below ~3.3eV. Al vacancies with charge states of -2, -1, and 0 dominate at smaller Fermi energies. Figure 5b shows comparable data at a pO_2 of 10^{-31} atm.

As the bulk defect calculations show, in the event that vacancies dominate point defect equilibrium (usually assumed for Al_2O_3), the Fermi level is close to where the

oxygen and Al vacancy lines cross (the vertical lines in Fig. 5), recognizing that the concentrations of oxygen and Al vacancies must be (nearly) in the ratio of 3:2 for charge neutrality (this assumes non-stoichiometry in Al_2O_3 is negligible). It is the condition of local charge neutrality that then determines the actual Fermi level, ~1.4eV at a pO_2 of 0.2 atm and ~3.3eV at $pO_2 = 10^{-31}$ atm near the scale/metal interface. However, if the Fermi energy is sufficiently close to the valence band edge, it may be possible for the charges present on V_{Al} defects to be compensated by holes in the valence band rather than by ionic point defects.

These figures also suggest a *p-n* electronic transition somewhere in the interior of the scale, depending on the number and mobilities of the electrons and holes. The very high electrical resistivity of Al_2O_3 scales (and Al_2O_3 ceramics) arises from the small number of charge carriers, as will now be discussed.

The Schottky energy for Al_2O_3 is so large, 3.5-4.0 eV per defect depending on temperature [33], that the native oxygen and Al vacancy concentrations are quite low, $\sim 10^{-8}$ or smaller. As shown by the construction in Fig. 5a at a pO_2 of 0.2 atm, and assuming Boltzmann statistics, a small fraction (0.035) of V_{Al} will be doubly, rather than triply ionized, and available for hole transport.

Near the scale/metal interface (Fig. 5b), electrons, rather than holes, will dominate charge transport. As shown in Fig. 5 of ref. [33], the electron density associated with the defect state is strongly localized on the oxygen vacancy. There is a relatively large fraction of singly charged oxygen vacancies available, with $V_O^{\bullet\bullet}/V_O^{\bullet}$ being 0.43 according to the self-consistent calculation of defect concentrations at a pO_2 of 10^{-31}. (Fortunately, differences in calculated DFT energies of importance here are subject to much smaller

uncertainties than absolute energy values and will not affect this finding.) This conclusion of transport involving oxygen and Al vacancies is unlikely to be affected by low levels of impurities in the scale—Ni^{2+} for Al_2O_3 scales on Ni-base alloys for example—because aliovalent impurities in Al_2O_3 must be present in hundreds of ppm quantities before they affect the Fermi level [33]. Furthermore, a recent atom probe tomography study with near- atomic resolution of an Al_2O_3 scale on a Pt-modified NiAl bond coat alloy showed the scale to be remarkably free of impurities [35].

Turning now to the electrical properties of Al_2O_3 scales, these are very difficult to determine with confidence. The Wagner approach leading to eqns. (6) and (7) for the electrochemical potential across the scale makes the assumption of zero total current, *I,* through the scale, the ionic current being exactly balanced by electron or hole currents. If inert conducting probes are placed across the scale, connected to a battery or even merely used to short-circuit the conducting pathways through the scale, this assumption no longer holds. In fact, it is easy to show that by relaxing the zero-current assumption, the left-hand side of eqn. (6) is modified from $\{V\}$ to $\{V + \langle \sigma^{-1} \rangle I\}$, where $\langle \sigma^{-1} \rangle$ is the mean inverse total conductivity of the scale and I the current. At the same time, the oxidation rate, eqn. (7), becomes

$$J = \frac{\sigma}{12} t_i (\nabla \mu_O - 2\nabla V). \qquad (10)$$

If the scale is short-circuited, the voltage difference, *V*, becomes zero, and the oxidation rate should increase by a factor $1/t_e$. Conversely, by applying a positive voltage to the outside of the scale, the oxidation rate should be retarded to zero when the voltage reaches one half of the difference in chemical potential of oxygen across the scale,

equivalent to $-\Delta G_{Al_2O_3}/6$. This makes sense, inasmuch as such an applied voltage would be attracting the migrating oxygen ions back to the outside and repelling aluminum ions back towards the metal.

Sheasby and Jory [32] attempted to measure the voltage developed by the scaling reaction, and noted the difficulties of the measurements; they were, however, able to show that a voltage applied across a scale could either dramatically retard or accelerate the oxidation rate, depending on the magnitude of the voltage.

The most reliable data on the electrical properties of Al_2O_3 scales appear to be those from Balmain and Huntz [16], who measured the transference number at 1100˚C of a ~2μm Al_2O_3 scale formed on β-NiAl in pure O_2 at 1100˚ C as a function of pO_2. The most important findings from their work were that the transference number was ~ 0.1 at the scale/gas interface, decreased to a minimum at a pO_2 of ~10^{-10} atm, and then rose to nearly 0.6 at the scale/metal interface, i.e., they showed a *p-n* ionic transition in the scale at a pO_2 of ~10^{-10} atm. They also calculated the oxygen chemical potential, μ_0, as a function of position in the scale, and suggested that μ_0 increased monotonically from the scale/metal interface nearly to the scale/gas interface, as is shown schematically in Fig.1.

As an interesting comparison, Wada *et al*. [15] extrapolated their high temperature ($\geq$1600 ˚C) permeability data acquired on dense Al_2O_3 ceramics to 1100˚C, and assuming oxygen pressures at the two surfaces of the scale of 1 atm and 10^{-28} atm (appropriate for a FeCrAl alloy at this temperature), calculated the variation of μ_o and μ_{Al} and the variation of δD_{gb}^{O} and δD_{gb}^{Al} across a growing Al_2O_3 scale. The chemical potential profiles were much flatter than the profile calculated by Balmain and Huntz [16]. It appears that improved data on electrical properties of Al_2O_3 scales, and

how μ_o and μ_{Al} vary across a growing scale, is essential for further progress in understanding the electrochemical properties of growing Al_2O_3 scales and the atomistic mechanisms involved in scale formation.

III. Line Defects and the Growth of Al_2O_3 Scales

3.1 Vacancy Creation/Annihilation

Vacancy production/annihilation at both the scale/gas and scale/metal interfaces are essential aspects of the growth of Al_2O_3 scales. Pieraggi, Rapp, and Hirth, henceforth PRH, have convincingly argued that line defects –interface dislocations, interface ***disconnections*** (described below), and surface ledges --are the sites where such production/annihilation take place [36,37]. We briefly discuss their point of view here, but note there are several significant complexities of Al_2O_3 scale formation compared to the simpler cases they considered.

PRH began by assuming that all scale/metal interfaces are semi-coherent, the misfit dislocations at the scale/metal interface playing an important role in cation vacancy annihilation and anion vacancy formation. Is this a good assumption for Al_2O_3 scales?

There have been a number of studies of the transient oxidation of both β-Ni(Al,Cr) and γ'-Ni_3(Al,Cr) alloys that speak to this point [38-41]. Well-defined orientation relationships are generally reported between the transition aluminas and their substrates. Subsequent transformation to the stable α- Al_2O_3 polymorph involves either nucleation at the scale/metal interface [39,40] or nucleation at the scale/gas interface [38]. In either case, close-packed planes in the transition aluminas are invariably parallel to close packed planes in the nucleated α-Al_2O_3.

The α-Al_2O_3 scale/metal interfaces have been reported to be incoherent [38], but previous high resolution transmission electron microscopy by our group [42] found a well-defined misfit dislocation structure between basal planes of α-Al_2O_3 and <101> oriented grains in a β-Ni(Al,Cr) alloy. More work of this type is clearly needed, but for present purposes, the PRH assumption of semi-coherent interfaces will be used as a working hypothesis for Al_2O_3 scale formation and growth.

The various line defects considered by PRH play different roles in the scaling reaction, depending on the species dominating scale growth. Consider anion transport first. New oxide formation will occur at the scale/metal interface, with annihilation of oxygen vacancies at ledges in the scale/gas interface, as described by eqn. 4. At the scale/metal interface, Al atoms of the metal must be converted to Al ions in the scale, with concurrent production of oxygen vacancies (eqn. 5). The flux of oxygen ions arriving from the scale/gas interface will form new oxide at this interface, which requires translation of ***interface disconnections***. These linear interface defects are ledges in the scale/metal interface, which are characterized by a step height, h, and a dislocation Burgers vector $\boldsymbol{b}$, the dislocation character of the defect accounting for its long range strain field [36]; as is usual, $\boldsymbol{b}$ defines the displacement associated with its motion.

The annihilation of the metal vacancies created by reactions (2) and (5) at the scale/metal interface can occur by climb of misfit dislocations away from the interface. Such climb of interface dislocations into the metal would normally produce a large local stress, as these interface dislocations are present to minimize the energy of the semi-coherent interface. The misfit dislocation spacing must therefore change, or be restored by glide of lattice dislocations from the metal to the interface by the Pieraggi-Rapp (PR)

process [43]; the climb of misfit dislocations away from the interface, followed by the PR process essentially constitutes a Bardeen-Herring climb source at the interface [37].

For scale growth by outward diffusion of Al, there is no difficulty creating cation vacancies at ledges at the scale/gas interface, but the same issue of how to annihilate Al vacancies at the scale/metal interface exists. PRH suggested the same resolution -- climb of misfit dislocations into the metal, with the return of lattice dislocation to the interface via the PR mechanism.

3.2 The Mechanism of Enhanced Grain-Boundary Diffusion

In addition to concerns with electron and hole availability (eqns. (1) to (5)), one major difference between Al_2O_3 scale formation and scaling reactions studied previously is the overwhelming dominance of grain-boundary diffusion at the temperatures of interest (i.e. > 900˚C). It has been generally assumed that such enhanced grain-boundary diffusion is similar to lattice diffusion, i.e., it involves random walk jumping of point defects (vacancies in the case of lattice diffusion in Al_2O_3), the enhancement (a factor of 10^6 or more) arising from the more open geometries of random high-angle grain boundaries. However, there are major problems with this point of view.

Firstly, the more open geometry of the grain boundary would be expected to significantly reduce the activation energy for grain-boundary diffusion, whereas literature data [8,11,30] and data to be shown in Fig. 9a suggest that the activation energy for the short-circuit diffusion process can be comparable to or even greater than that for lattice diffusion. Secondly, there is near-universal agreement in the ceramics literature that grain boundaries in polycrystalline ceramics, including Al_2O_3, are perfect sources and sinks for point defects (vacancies and interstitials). The usual interpretation is that when (say) a

vacancy is annihilated by jumping into a grain boundary, all of the grain-boundary cations and anions slightly adjust their positions to eliminate some of the free volume associated with the vacancy. In other words, the vacancy becomes *delocalized*. The ability of boundaries to transform point defects into delocalized atomic rearrangements renders the very idea of point defects at grain boundaries problematic. It also suggests that the mechanism of grain-boundary diffusion is cooperative and should not be viewed as point-defect hopping.

Heuer, in his recent review of oxygen and aluminum diffusion in Al_2O_3 [8], noted that the large magnitude of published values for Do and Q (the pre-exponential and activation energy) for oxygen grain boundary diffusion in Al_2O_3 are difficult to understand in terms of basic random walk diffusion theory involving simple jumping of vacancies or interstitials in a disordered region adjacent to a grain boundary. He suggested instead that grain boundary diffusion "could occur via glide/climb of grain boundary dislocations, grain boundary ledges, and other structural (linear) defects". More recently, Hirth [44] suggested that such enhanced grain boundary diffusion involves migration of grain-boundary disconnections. It follows that vacancy production/annihilation must occur at jogs on these disconnections. By analogy with lattice dislocations, the migration must involve repeated double kink nucleation of the disconnections. Furthermore, coarsening of the scale microstructure is an essential aspect of scale growth (see Fig. 1 of ref. [11] and ref. [19]) and most likely occurs by the motion of grain boundary disconnections.

The extensive literature on interface disconnections, summarized recently in ref. [45], has been mostly concerned with rational low index interphase interfaces, but the

notion that disconnection line defects exist in random high angle general grain boundaries and can mediate both grain-boundary migration and enhanced grain-boundary diffusion is mechanistically very appealing. As any random high-angle grain boundary can be considered as defining a CSL with a very large Σ value, the corresponding DSC Burgers vectors would be correspondingly small.* The basic idea of disconnection-mediated enhanced grain-boundary diffusion as applied to scale growth is shown in the sketches in Figs. 6 and 7. We consider cation transport first (Fig. 6).

The first step is for oxygen molecules to dissociate, the individual atoms absorbing at surface steps or surface ledges, where they form lattice oxygen ions – new oxide – and the requisite number of Al vacancies (Fig. 6a). These vacancies could in principle migrate by lattice diffusion to the scale/metal interface, as is generally the case in the growth of NiO at elevated temperature (>1000˚C) [27], but the lattice diffusion kinetics in Al_2O_3 are too sluggish. Rather, the newly formed Al vacancies can migrate by surface diffusion to the nearest grain boundary, where they are annihilated at a jog on a grain-boundary disconnection. The annihilation of the Al vacancy transfers some of the vacancy volume and all of the vacancy charge to the now-negatively charged jog. Continued oxide growth would then involve further creation of lattice oxygen ions, with continuing surface diffusion of Al vacancies to grain-boundary disconnections, where they are annihilated. Migration of grain boundary disconnections containing these negatively charged jogs towards the scale/metal interface provides the requisite mass

* DSC, regarded as an acronym for the terms "Displacement Shift Complete" or "Displacement Symmetry Conserving", is the lattice formed by the union of the two sets of lattice vectors belonging to the crystals on either side of the boundary, while the CSL or "Coincident Site Lattice" is the lattice formed by the intersection of those two sets.

transport for the scaling reaction (Fig. 6b) and is the grain boundary equivalent of lattice diffusion of Al vacancies.

At the scale/metal interface, Al vacancies are then reconstituted and undergo interfacial diffusion to the closest interface disconnection (Fig. 6c), where they are annihilated (eqn. 2), the metal vacancies thus produced being injected, via climbing misfit dislocations, into the metal substrate (Fig. 6d). Glide of lattice dislocations in the metal towards the scale/metal interface (the PR mechanism) is necessary to ensure the appropriate misfit dislocation spacing (Fig. 6d).

A similar process is envisioned for anion transport (Fig. 7). Anion vacancies are created at disconnections at the scale/metal interface (Figs. 7a and b), and migrate to the nearest grain boundary, where their annihilation on a grain boundary disconnection creates positively charged grain-boundary jogs (Fig. 7c). These can migrate along grain boundaries of the scale to the scale/gas interface, where oxygen vacancies can be recreated, and undergo surface diffusion to surface ledges, where they react with absorbed oxygen atoms to form new O_O^x lattice sites (Fig. 7d).

This proposed mechanism provides a ready explanation for the well-documented [9,10] countercurrent grain-boundary transport of both oxygen and Al in Al_2O_3 scales formed on NiCrAls and FeCrAls. The formation of "internal" oxide with its resulting lateral strain then has to be understood in terms of divergences in the fluxes of these charged jogs, enabled by their spontaneous generation within the grain boundary. Disconnections containing positively charged jogs migrating towards the scale/metal interface on a particular grain boundary could react with disconnections containing negatively charged jogs migrating towards the scale/gas interface on the same boundary

to annihilate "molecules" of Al_2O_3, and the reverse process of charged kink-pair generation might generate new crystal. Actually, these mechanisms are still speculative and the precise role of charged jogs on grain boundary disconnections in the development of oxidation-induced stresses during Al_2O_3 scale growth requires further discussion.

As was discussed in the "New Perspective" paper [11], steady state oxidation-induced compressive stresses in scales grown on Ni-base and Fe-base alloys are in the 100-200 MPa range but become tensile and of a similar magnitude upon RE additions. In the context of new oxide forming from divergence of ion fluxes within the scale, in order to generate compressive stresses, the molar volume of the newly -formed Al_2O_3 must be (at least) slightly greater than the free volume of the vacancies that are annihilated.

In addition to the possible role of REs inhibiting Al grain-boundary diffusion by affecting the density of near-band edge grain-boundary donor and acceptor states, the REs probably also hinder the migration of negatively charged grain-boundary disconnections. This is similar to solute atoms hindering the glide motion of lattice dislocations and will of course further limit internal oxide formation. Finally, the positive (tensile) strains measured in Al_2O_3 scales grown on RE-containing alloys [46] must arise, at least in part, from the loss of free volume accompanying annihilation of oxygen vacancies on grain boundary disconnections.

There are several interesting consequences of the model just discussed. Firstly, line defects showing dislocation contrast should be present in grain boundaries of the scale. Fig. 8a, taken from Smialek's Ph.D. thesis [47] but not previously published, shows just such defects. Secondly, ledge defects should be present in grain boundaries in Al_2O_3 scales, as well as in grain boundaries in Al_2O_3 ceramics. Fig. 8b shows a series of

such ledge defects in an oxide scale on a FeCrAlY (Kanthal AF) oxidized at 1200°C for 50 hours in air and water quenched. (Similar grain boundary disconnections have been published recently by Yu *et. al.* in a Hf-doped Al_2O_3 polycrystal [48].) Finally, inasmuch as any particular grain boundary will contain disconnections with unique, i.e., different, values of h and $\boldsymbol{b}$, their mobility under the driving force of the free energy involved in the oxidation reaction (eqn. (8)) will be different. This will manifest itself as differences in δD^{O}_{gb} and δD^{Al}_{gb} for different grain boundaries in Al_2O_3 scales. All random high angle grain boundaries may not be equal!

Recent ^{18}O and ^{26}Al tracer studies using SIMS and TOF-SIMS [30,49] on both Al_2O_3 bicrystals and Al_2O_3 polycrystals show just such behavior. In the bicrystal work [30], differences in δD^{O}_{gb} of up to 10^3 were reported on similarly prepared bicrystals with different CSL Σ values and different boundary planes; the diffusion activation energy likewise varied from 540 to 840 kJ/mol, up to ~1.5x that for lattice diffusion. These values are clearly inconsistent with the material science "rule of thumb" that activation energies for grain boundary diffusion should be about 0.5x that of lattice diffusion. In the case of polycrystalline Al_2O_3, details of which are to be reported elsewhere [49], the enhancements were even larger than in the bicrystals, increasing by a factor of 10^6-10^7 compared to lattice diffusion, with adjacent grain boundaries having δD^{O}_{gb} differences up to several orders of magnitude (Fig. 9a). The important implication is that an activation energy for oxygen grain-boundary diffusivity cannot be derived from average data at different temperatures. Rather, studies of individual grain boundaries at different temperatures are necessary to derive activation energies. Fortunately, as shown in the ^{18}O TOF-SIMS image of Fig. 9b, the dense sintered polycrystalline Al_2O_3 used for the

quantitative data in Fig. 9a has a grain size of ~10μm, which makes such studies of individual grain boundary diffusivities tractable, given the high spatial resolution of the TOFS-SIMS apparatus used for this work, ~100nm. In fact, we find the activation energy for oxygen grain boundary diffusion for individual boundaries to vary from 2.9 to 13eV[49]!

The δD_{gb}^{Al} tracer data are more limited and data acquisition is not conducive to measuring diffusivities of individual boundaries because of the very low concentration of the long-lived ^{26}Al tracer used; however, the data clearly show that δD_{gb}^{O} and δD_{gb}^{Al} are comparable, consistent with the observation that both inward oxygen and outward Al grain-boundary diffusion can occur during Al_2O_3 scale formation on NiCrAl and FeCrAl alloys. Note again that the pre-exponential and activation energy for δD_{gb}^{Al} are so large that they are not consistent with a point defect diffusion mechanism. Further study of ^{26}Al diffusion in Al_2O_3 grain boundaries is underway.

Finally, the proposed model just discussed allows for conventional interpretations of defect equilibria and, hence, rationalization of the oxygen permeability results of Kitaoka *et al*. [12-15]. Specifically, equations (1) and (3) remain valid representations of the role of O_2 in creating ionic and electronic defects in the Al_2O_3 scale.

IV Summary and Conclusions

The atomistic processes involved in the growth of Al_2O_3 scales have been reconsidered at a fundamental level. The scaling reaction has been treated in the framework of Wagner's classic theory of theory of metal oxidation, emphasizing the importance of the electrical properties of Al_2O_3 scales on scale growth. This in turn

requires consideration of the electronic band structure of polycrystalline Al_2O_3. Both electrons and holes must be involved in the scaling reactions, and we suggest that electrons migrate through the scale while hopping on and off singly charged oxygen vacancies, $V_O^{\bullet}$, while holes hop off and on doubly charged Al vacancies, V_{Al}''. The fractional concentration of doubly charged Al vacancies in the bulk has been calculated on the basis of formation energies derived from DFT calculations, as a function of pO_2, and is significant near the scale/gas interface, namely 0.035 at T=1250K; hole conduction dominates in this region of the scale. An even larger fraction of singly charged oxygen vacancies is present near the scale/metal interface, 0.435, and electron conduction probably dominates at the low pO_2 there. The role of the grain boundary as a pathway for electron and hole conduction is still unknown.

Growth of Al_2O_3 scales occurs entirely by grain-boundary diffusion, and is particularly interesting for NiCrAl and FeCrAl alloys lacking reactive element additions, where simultaneous inward diffusion of oxygen and outward diffusion of Al is known to occur. Lateral stresses will naturally arise in the growing scales due to divergence of the fluxes of ions and consequent deposition or dissolution of crystal; this phenomenon might be characterized as electrochemically driven strain.

A mechanism of enhanced grain-boundary diffusion during Al_2O_3 scale growth has been suggested; the enhancement is ***not*** a result of easier jumping of compact point defects, i.e., vacancies and/or interstitials, in the more open geometry of random high high-angle grain boundaries, but rather involves migration of grain-boundary disconnections containing positively charged and negatively charged jogs. These disconnections are interfacial ledge defects characterized by a step height, *h*, and a

Burgers vector, ***b***, which accounts for the long long-range strain field of the ledge defect and defines the displacement associated with disconnection migration. Dislocation-like defects should be visible in scale grain boundaries with TEM. Further, measurable differences should be observed in grain boundary diffusivities in adjacent random high angle grain boundaries. Both of these last two predictions have been confirmed.

Acknowledgements

The research at CWRU and the Univ. of Pittsburgh was supported by the Office of Naval Research (ONR), Dr. David Shifler, Program Manager; while that at Imperial College, London was supported by The Leverhulme Trust grant F/07058/BS and the Office of Naval Research Global. This work made use of facilities provided by the Imperial College London High Performance Computing Service. Via our membership of the UK's HPC Materials Chemistry Consortium, which is funded by the EPSRC (EP/F067496), this work also made use of the facilities of HECToR, the UK's national high-performance computing service, provided by UoE HPCx Ltd. at the University of Edinburgh, Cray Inc. and NAG Ltd., and funded by the Office of Science and Technology through EPSRC's High End Computing Programme.

NDMH acknowledges the support of a Leverhulme Early Career Fellowship and EPSRC grant EP/G05567X/1. AHH acknowledges useful e-mail correspondence with J.P. Hirth and R.A. Rapp on the importance of disconnections in scaling reactions, and AHH, WMCF, and MWF acknowledge useful discussions with A. Atkinson on the electrical properties of Al_2O_3 in regard to Al_2O_3 scale formation. J.P. Hirth specifically suggested that enhanced grain grain-boundary diffusion was mediated by grain-boundary disconnections.

References

1) F.H. Stott, High. Temp. Corros. Prot. Mater., Vol. 4 (Part 1), p 251-2, 1997
2) F.H. Stott, High. Temp. Corros. Prot. Mater., Vol. 4 (Part 2), p 19-32, 1997
3) S. Chevalier, Developments in High Temperature Corrosion and Protection of Materials, Edited by W. Gao, CRC Press, Boca Raton, FL, p 290-329, 2008
4) J. Jedlinski and G. Borchardt, Oxid. Metals, Vol. 36, p 317, 1991
5) P. Prescott and M.J. Graham, Oxid. Metals, Vol. 38, p 233, 1992
6) B.A. Pint and K.B. Alexander, J. Electrochem. Soc., Vol. 145, p 1819-1829, 1998
7) P.Y. Hou, J. Amer. Ceram. Soc. Vol. 86, p 660, 2003
8) A.H. Heuer, Journal of the European Ceramic Society, Vol. 28, p 1495-1507, 2008
9) W.J. Quadakkers, A. Elschner, W. Speier, and H. Nickel, Appl. Surf. Sciences, Vol. 52, p 271, 1991
10) R. Prescott, D.F. Mitchell, M.J. Graham, and J. Doychak, Corrosion Science, Vol. 37, p. 1341, 1995
11) A.H. Heuer, D.B. Hovis, J.L. Smialek and B. Gleeson, J. Am. Ceram. Soc, Vol. 94, p 146-153, 2011
12) S. Kitaoka, T. Matsudaira, and M. Wada, Materials Transactions, Vol. 50, p1023-1031, 2009
13) T. Matsudaira, M. Wada, T. Saitoh, S. Kitaoka, Acta Materialia, Vol. 58, p1544-1553, 2010
14) T. Matsudaira, M. Wada, T. Saitoh, S. Kitaoka, Acta Materialia, Vol. 59, p5440-5450, 2011
15) M. Wada, T. Matsudaira, and S. Kitaoka, Journal of the Ceramic Society of Japan, Vol. 119, p 832-839, 2011
16) J. Balmain and A.M. Huntz, Oxidation of Metals, Vol. 46, p 213-234, 1996
17) D. J. Young, D. Naumenko, L. Niewolak, E. Wessel, L. Singheiser, and W.J. Quadakkers, Materials and Corrosion, Vol. 61, p 838-844, 2010
18) T.A. Ramanayanan, M. Raghavan, and R. Petkovic-Luton, Mater. High. Temp., Vol. 20, p 261-271, 1984.

19) J. Smialek *et al.*, in preparation
20) C. Wagner, Z. Phys. Chem, Vol. B21, p 25, 1933
21) J.E. Harris, Acta Metall., Vol. 26, p. 1033-1041, 1978
22) R. Vale and R.E. Smallman, Phil. Mag., Vol. 36, p. 209-223, 1977
23) R. Francis and D.G. Lees, Mater. Sci. Eng., Vol. A120, p.97-99, 1989
24) S. Perusin, B. Viguier, D. Monceau, L. Ressier, and E. Andrieu, Acta Mater., Vol. 52, p. 5375-5380, 2004
25) A.H. Rosenstein, J.H. Tien, and W.D. Nix, Metall. Trans. A, Vol. 17A, p. 151-162, 1986
26) H.E. Evans, Mater. Sci. Technol., Vol. 4, p. 1089-1098, 1988
27) A. Atkinson, Reviews of Modern Physics, Vol. 57, p 437-470, 1985
28) R. H. French, J. Am. Ceram. Soc., Vol. 73, p 477-489, 1990
29) S.J. Clark, M.D. Segall, C.J. Pickard, P.J. Hasnip, M.J. Probert, K. Refson. And M.C. Payne, Z. Kristall., 220-597 (2005).
30) T. Nakagawa, H. Nishimura, I. Sakaguchi, N. Shibata, K. Matsunaga, T. Yamamoto and Y. Ikuhara, Scripta Materialia*, V*ol. 65, p 544-547, 2011
31) K.H. Hauffe and S.R. Morrison, High Temperature Gas-Metal Reactions in Mixed Environment, S.A. Jansson and Z.A. Foroulis, Eds, The Metallurgical Society of AIME, New York, p 33-62, 1973
32) J.S. Sheasby and D.B. Jory, Oxidation of Metals, Vol 12, p 527-539, 1978
33) N.D.M. Hine, K. Frensch, W.M.C. Foulkes, and M.W. Finnis, Phys. Rev. B, Vol.79, 024112, 2009
34) M. Choi, A. Janotti, C. G. Van de Walle, J. Appl. Phys. 113, 044510, 2013
35) K. Stitler, L. Viskani, G. Sundell, F. Liu, M. Thuvander, H-O Andrén, D.J. Larson, T. Prosa, and D. Reinhard, Oxidation of Metals, in press
36) J.P. Hirth, B. Pieraggi, and R.A. Rapp, Acta Metal. Mater., Vol. 43, p 1065-1073, 1995
37) B. Pieraggi, R.A. Rapp, and J.P. Hirth, Oxidation of Metals, Vol. 44, p 63-79, 1995
38) J. Doychak, J.L. Smialek, and T.E. Mitchell, Metallurgical Transactions, Vol. 20A, p 499-517, 1989

39) J. Doychak and M. Rühle, Oxidation of Metals, Vol. 31, p 431-452, 1988
40) E. Schumann and M. Rühle, Acta metal. Mater., Vol. 42, p 1481-1487, 1994
41) J.C. Yang, E. Schumann, I. Levin and M. Rühle, Acta. Mater., Vol. 46, p 2195-2201, 1998
42) L. Hu, D. Hovis and A.H. Heuer, Scripta Materialia, Vol. 61, p 157-160, 2009
43) B. Pieraggi and R.A. Rapp, Acta Metall., Vol. 36, p. 1281, 1988
44) J.P. Hirth, private communication, 2012
45) J.M. Howe, R.C. Pond, J.P. Hirth, Progress in Materials Science, Vol. 54, p 792-838, 2009
46) B. W. Veal, A. P. Paulikas, B. Gleeson, and P. Y. Hou, *Surf. Coat. Technol.*, Vol. 202, p 608 -612, 2007
47) J. Smialek, Ph.D. Thesis, Case Western Reserve University, Jan. 1981
48) Z. Yu, Q. Wu, J M Rickman, H.C. Chan, and M.P. Harmer, Scripta Materialia, Vol. 68, p. 703-706, 2013
49) T. Nakagawa, D. Hovis and A.H. Heuer, to be published

Figure Captions

1. Schematic drawing of the variation of oxygen chemical potential across a growing Al_2O_3 scale.
2. Schematic diagram of the band structure of polycrystalline Al_2O_3. The filled valence band contains mostly oxygen 2*p* states, the empty conduction band mostly hybridized Al 3*s*/3*p* states. For a stoichiometric oxide, the Fermi level, ε_F, is expected to be near the center of the (very large) single crystal band gap. States associated with grain boundary (GB) oxygen and Al ions extend into the gap, in close proximity to deep levels associated with oxygen and Al vacancies. These levels are shown (as is conventional for semiconductors) as donor states, $V_O^{\bullet}$, and acceptor states, V_{Al}'', ***after*** they have trapped an electron or hole, respectively.

3. (a) Electronic density of states (DOS) of a pristine $\Sigma 7\ \{4\bar{5}10\}$ symmetric tilt bicrystal grain boundary in Al_2O_3 and (b) after replacing one of Al atoms in the grain boundary core region with Y. The upper panels show the respective total DOS referenced to the bulk valance band maximum, which is indicated for the sake of clarity by the green vertical lines. The lower panels show the contributions of indicated species in the grain boundary ("GB") and the bulk ("Bulk") region deep within the grains. The shaded areas below the red curves indicate the occupied states.
4. Schematic views of the electric field across a growing Al_2O_3 scale; (a) and (b) show the limiting case where $\sigma_i>\sigma_e$ whereas (c) and (d) the opposite situation, where $\sigma_e>\sigma_i$. Further, (a) and (c) show the case for scale growth at the scale/metal interface (outward transport of oxygen vacancies ($V_O^{\bullet\bullet}$)), while (b) and (d) show the case for scale growth at the scale/gas interface (inward transport of Al vacancies (V_{Al}''')). Following Wagner [20], electron or hole transport must occur during scale growth. Inasmuch as the mobilities of both types of vacancies, and of electrons and holes will not be equal, an electric field will develop during the earliest stages of the oxidation reaction and persist during scale growth; these fields will cause tilting of the conduction band minimum, ε_{CBM}, and the valence

band maximum, ε_{VBM}, as well as the $V_O^{\bullet}$ and V_{Al}'' levels (see Fig. 2). The Fermi level, ε_F, is pinned at the scale/metal interface by its value in the metal and at the scale/gas interface by the V_{Al}'' level. Creation/annihilation of oxygen or Al vacancies can only occur at the scale/gas and scale/metal interfaces and involves the electrons and holes shown in eqns. 1, 2, 4 and 5 , which become trapped on oxygen and *Al* vacancies to form $V_O^{\bullet}$ and V_{Al}'', respectively. ε_g is the energy of the band gap.

5. Formation energies of oxygen and Al vacancies in various charge states as a function of the Fermi energy, ε_F. 1250K, pO_2 = 0.2 atm (a); $pO_2 = 10^{-31}$atm (b). All charge states are present at some concentration at any value of ε_F. V_{Al}''' is the dominant charge state for Fermi energies of 1 eV and above; V_{Al}'', V_{Al}', and V_{Al}^{x} dominate at lower Fermi energies. $V_O^{\bullet}$ is the dominant charge state for values of ε_F below 3.4 eV. At any $p(O_2)$, the actual Fermi level is determined by the Schottky equilibrium and is ~ 1.3 eV at $p(O_2)$ = 0.2 atm and ~ 3.3 eV at $p(O_2) = 10^{-31}$ atm; it is determined by the intersection of the oxygen vacancy and Al vacancy curves (the vertical lines), where the concentrations are (nearly) in the ratio of 3:2 (this insures point defect equilibrium). There is a sizeable concentration of V_{Al}'' at 0.2 atm, shown by the dotted extension of the V_{Al}'' curve, and equal to 0.035 V_{Al}''', assuming Boltzmann statistics; Al_2O_3 will thus exhibit *p*-type electronic conductivity near the scale/gas interface. Near the scale/metal interface (b), $V_O^{\bullet}/V_O^{\bullet\bullet}$= 0.435 and Al_2O_3 will show *n*-type electronic conductivity.

6. Schematic view of Al_2O_3 scale formation involving cation grain boundary diffusion mediated by grain boundary disconnections. (a) shows new oxide forming at the scale/gas interface at a surface ledge. Al vacancies created by eqn. 1 migrate by surface diffusion to the closest grain boundary, where the vacancy is annihilated at a jog on a disconnection, forming a negatively charged grain boundary jog (b). (c) shows the situation after the disconnection has migrated to the scale/metal interface, and an Al vacancy has reformed and migrated to an interfacial disconnection. The final step in oxide formation is for the reaction

described by eqn. 2 to occur (d). Vacancy injection into the metal is accomplished by climbing misfit dislocations, which are resupplied to the interface by glide of lattice dislocations in the substrate (the Pieraggi-Rapp process [43]).

7. Schematic view of Al_2O_3 scale formation involving anion grain boundary diffusion. The first step (a) is the formation of an oxygen vacancy at the scale/metal interface via eqn. 5. (The necessary vacancy injection into the metal again involves the Pieraggi-Rapp process.) The anion vacancy migrates via interfacial diffusion to the closest grain boundary at the scale/metal interface (b), where it is annihilated and forms a positively charged oxygen grain boundary jog, which migrates to the scale/gas interface. At this interface, the oxygen vacancy is reconstituted and migrates to the closest surface ledge (c), where eqn. 4 can occur.

8. (a) TEM micrographs showing features exhibiting dislocation contrast in an Al_2O_3 scale formed on a Ni15Cr24Al alloy, oxidized at 1100º C in air for 20h. The image shows a special low angle grain boundary for a cluster of $\{10\ \bar{1}\ 1\}$ oriented grains in an array of otherwise featureless high angle boundaries. The image can be analyzed as two orthogonal Moiré patterns, consistent with interference caused by two pairs of slightly rotated diffracted **g** vectors. The $\Delta\mathbf{g}$ vectors determine the orientations and spacings of the Moiré fringes (1.5 and 2.4 nm), consistent with the image features. The ~10 nm steps in the array of the Moiré fringes are clearly interface dislocations. Reference [47]. (b) Low magnification image of an Al_2O_3 scale formed on FeCrAlY (Kenthal AF) oxidized at 1200°Cin air for 50 hours and water quenched. The low magnification image reveals a conventional scale microstructure; the arrowed features in the HREM image in (c) are clearly disconnections in this random high angle grain boundary. (d), (e), and (f) are electron diffraction patters, showing that the grain on the left in (c) is oriented to a $[2\bar{2}01]$ zone axis orientation, while the grain to the right is ~2° from a $[20\bar{2}1]$ zone axis orientation. The orientation of the left and right hand grains in (c) are shown in the stereographic projection insert in (c), which is centered on $[20\bar{2}1]$. (g) XEDS spectra of two 13x75nm areas around the grain boundary in question. Area 1 is from the grain boundary itself, and shows enrichment of Ti, Zr, and Y.

Area 2 is from a region of the grain removed from the grain boundary and shows no detectable Ti, Zr, or Y.

9. (a) Arrenhius plot of oxygen and Al lattice and grain boundary diffusion in Al_2O_3. References for oxygen and Al lattice diffusion can be found in refs. [8], [11], and [49]. The data for oxygen and Al grain boundary diffusion, determined using ^{18}O and ^{26}Al tracers, is from ref. [49], and assumes the grain boundary width, δ, is 1 nm. (b) ^{18}O TOF-SIMS image with high spatial resolution, ~100nm. The large differences in δD_{gb}^{O} shown in a) are not due to experimental scatter but rather to differences in δD_{gb}^{O} in adjacent grain boundaries in a fully dense sintered Al_2O_3 polycrystal with a ~10μm grain size. Because of the large differences in grain boundary diffusivities, determination of an activation energy for oxygen grain boundary diffusion requires study of a single boundary at different temperatures, especially for those boundaries sharing a common grain. The ^{26}Al grain boundary diffusion data is more limited but shows that δD_{b}^{O} and δD_{b}^{Al} are comparable, i.e. the enhancement compared to lattice diffusion is significant for both species, but more so for oxygen. See ref. [49] for further details.

Figure 1

Variation of Oxygen Chemical Potential Across a Growing Al_2O_3 Scale

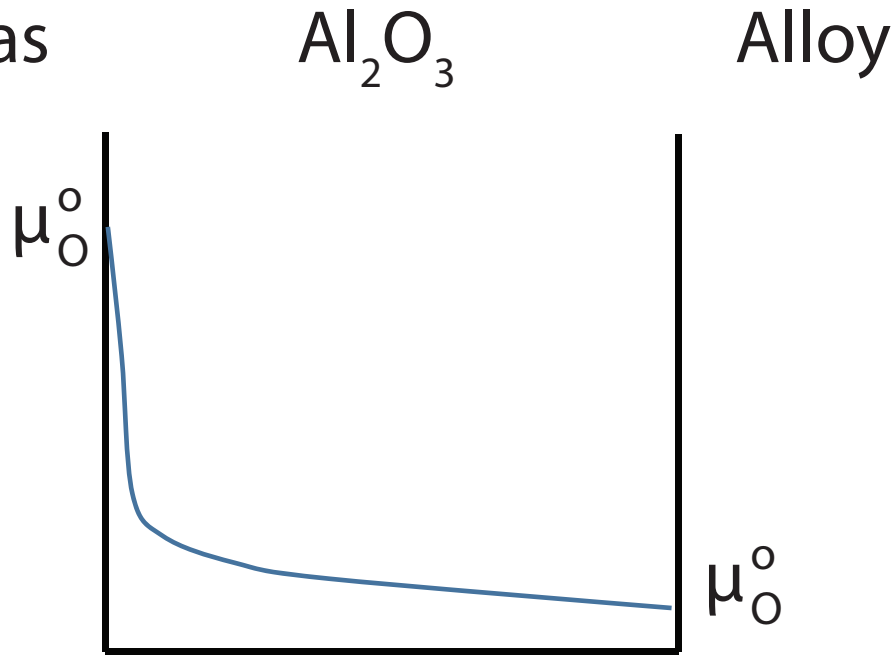

Figure 2

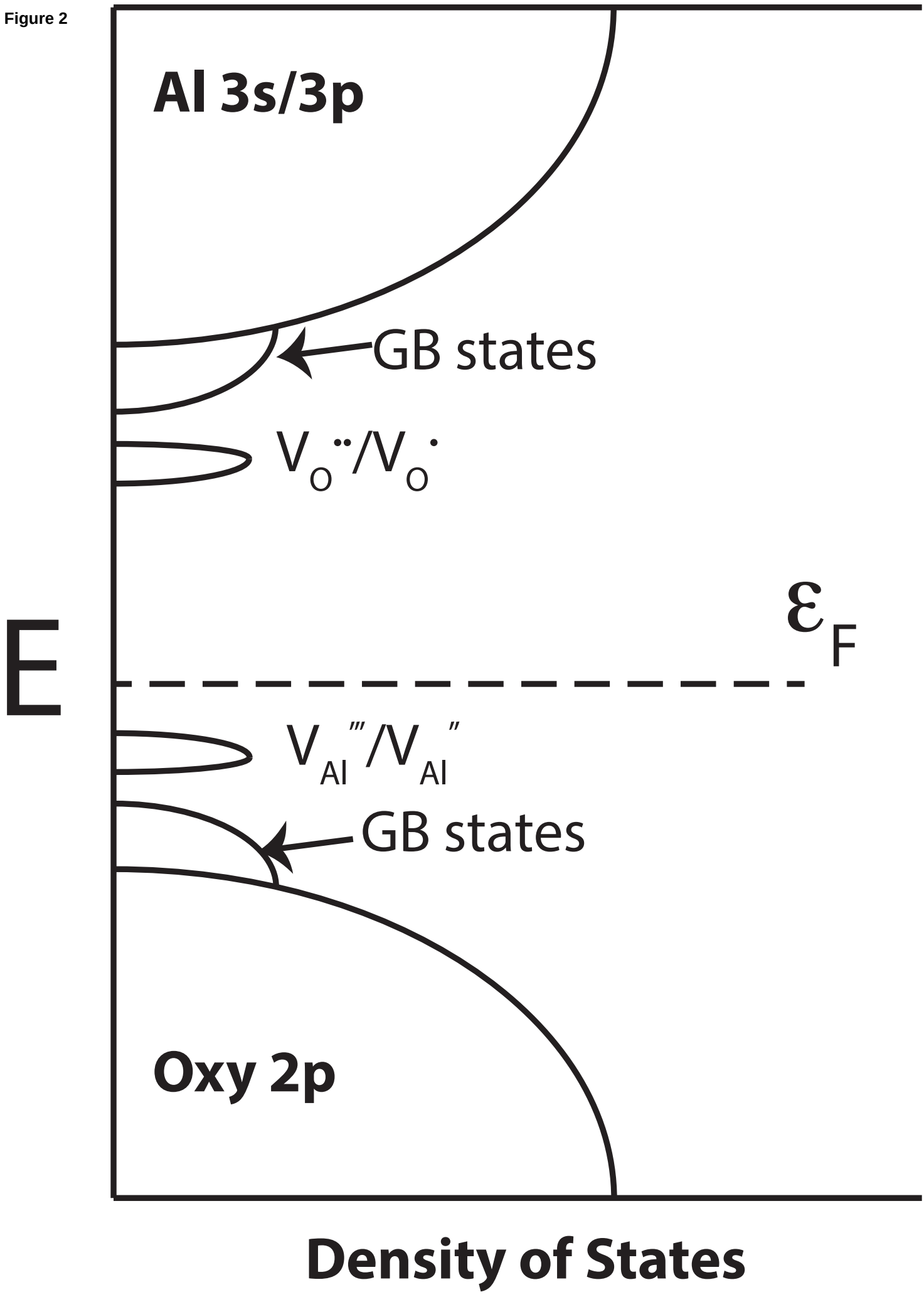
Al 3s/3p
GB states
$V_O^{\cdot\cdot}/V_O^{\cdot}$
E
ε_F
$V_{Al}^{'''}/V_{Al}^{''}$
GB states
Oxy 2p
Density of States

Figure 3

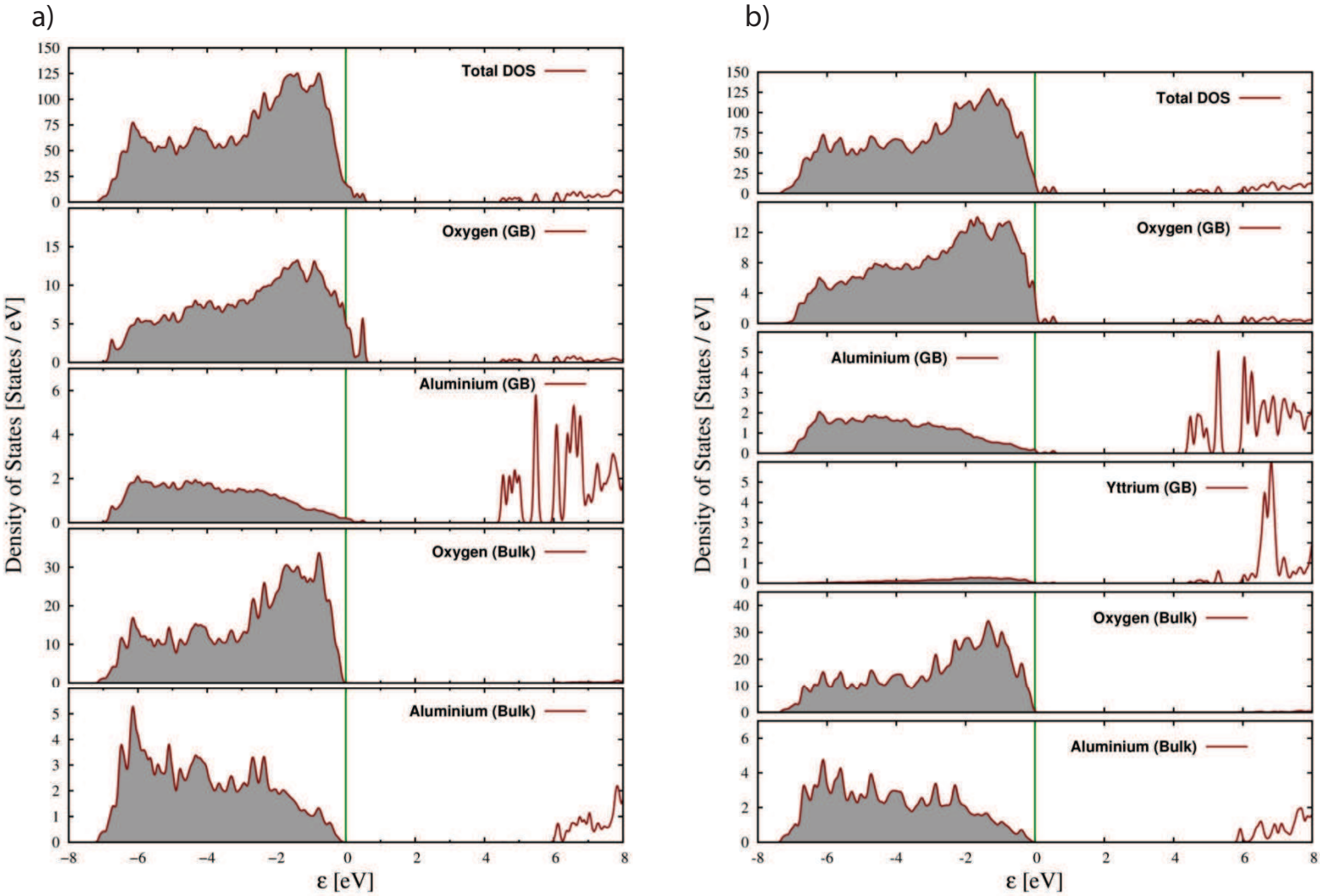
a)
b)
Total DOS
Oxygen (GB)
Aluminium (GB)
Yttrium (GB)
Oxygen (Bulk)
Aluminium (Bulk)
Density of States [States / eV]
ε [eV]

Figure 4

a)

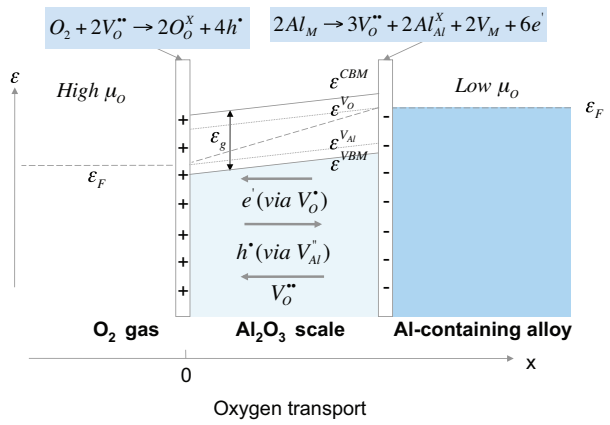

b)

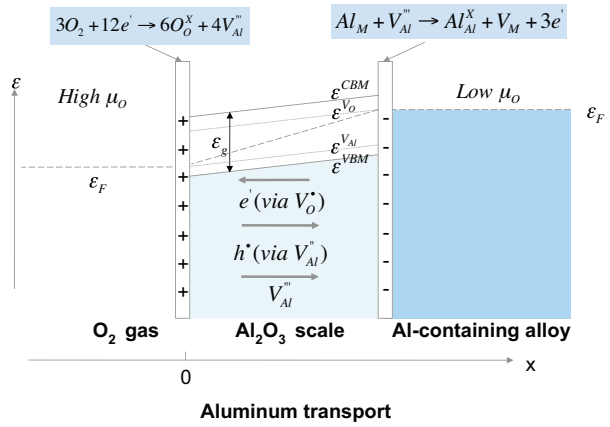

c)

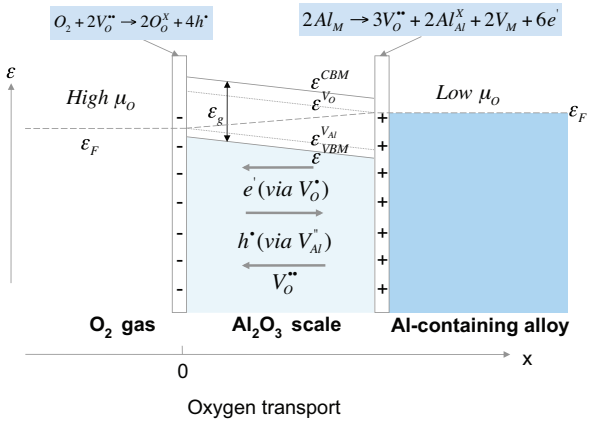

d)

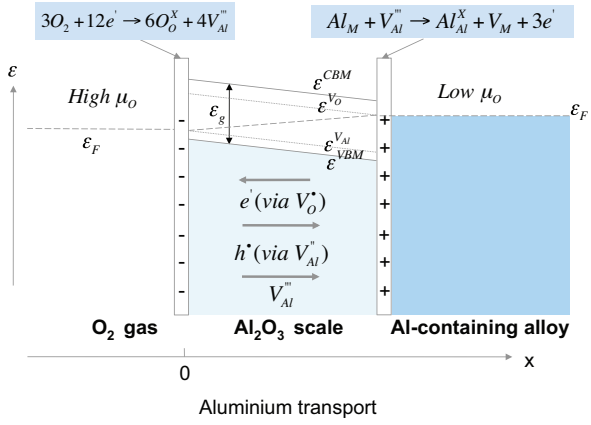

Figure 5

a) Formation Energies of Oxygen and Al Vacancies: 1250K, $p(O_2) = 0.2$ atm

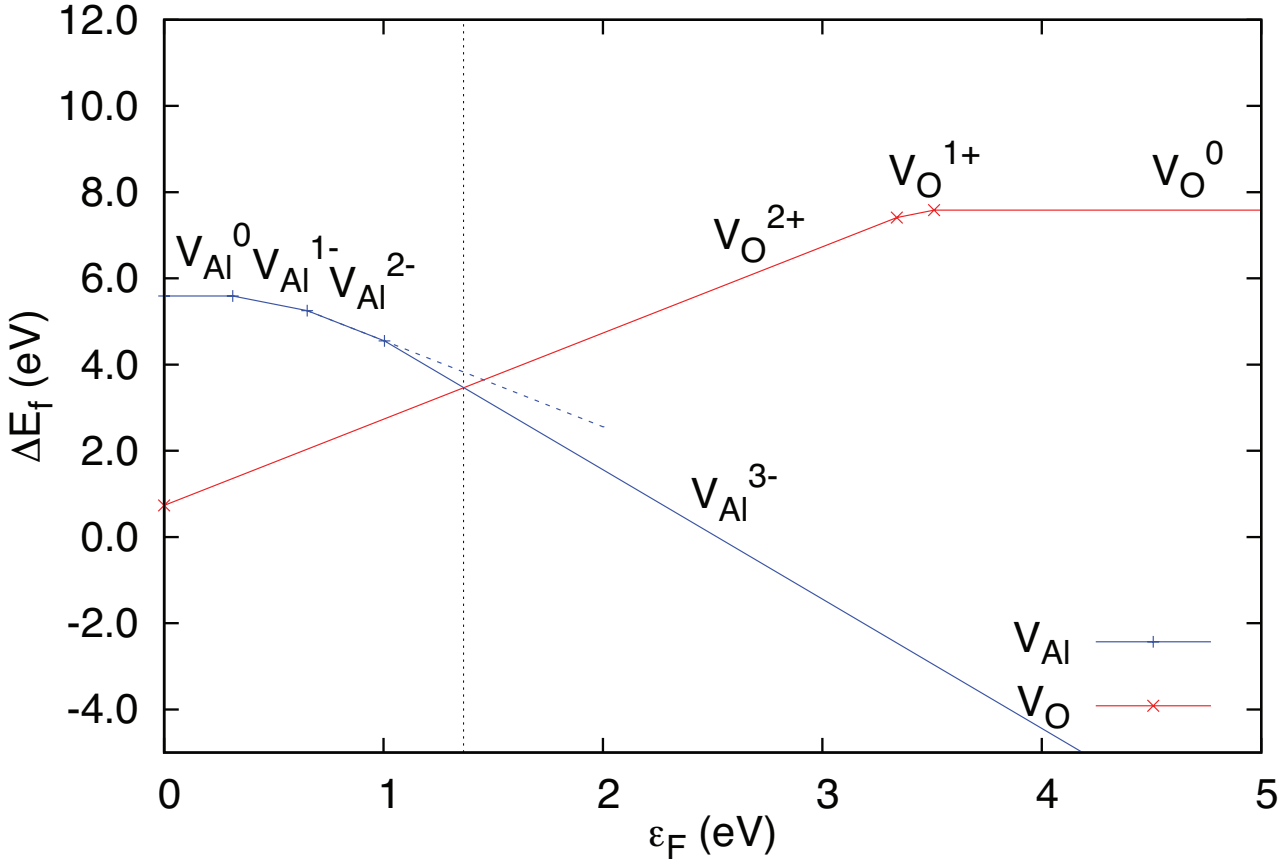

b) Formation Energies of Oxygen and Al Vacancies: 1250K, $p(O_2) = 10^{-31}$ atm

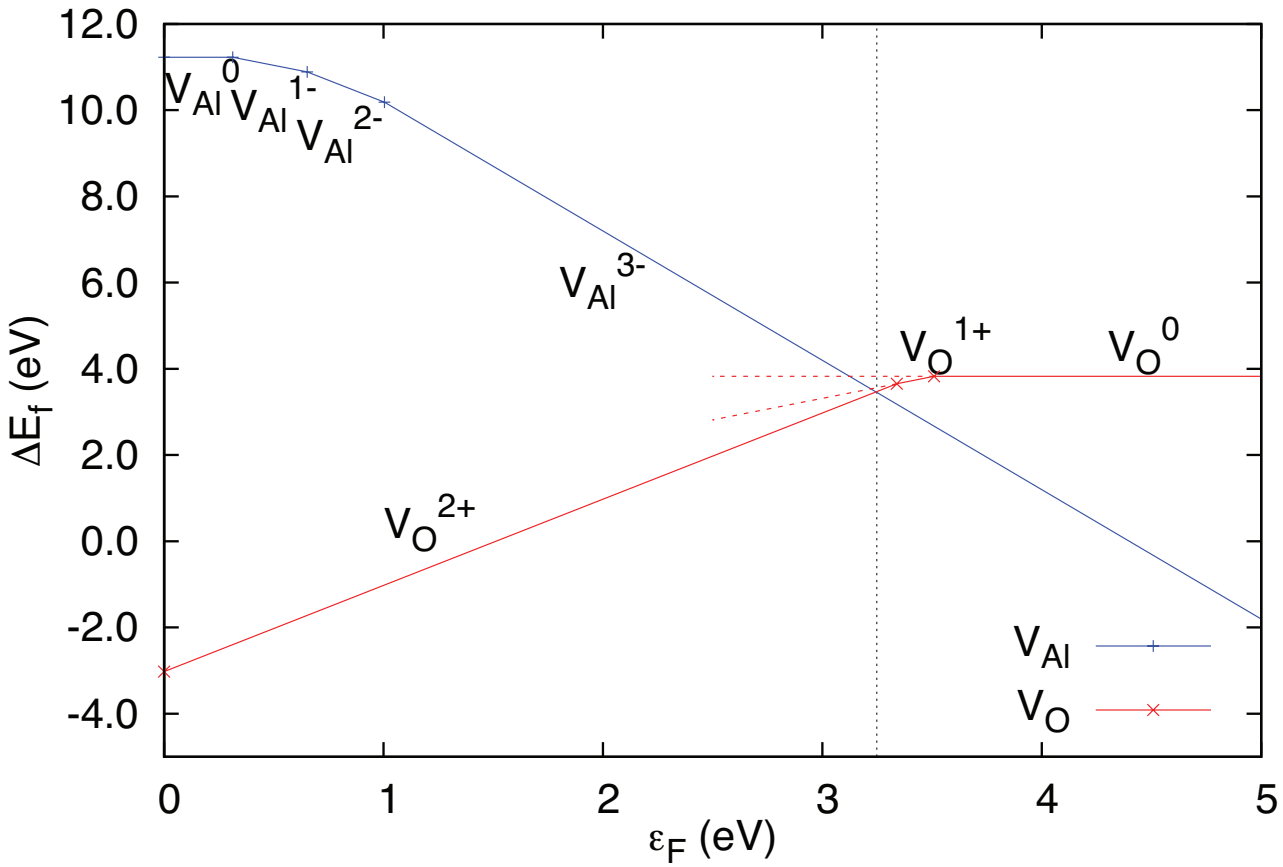

Figure 6

a)

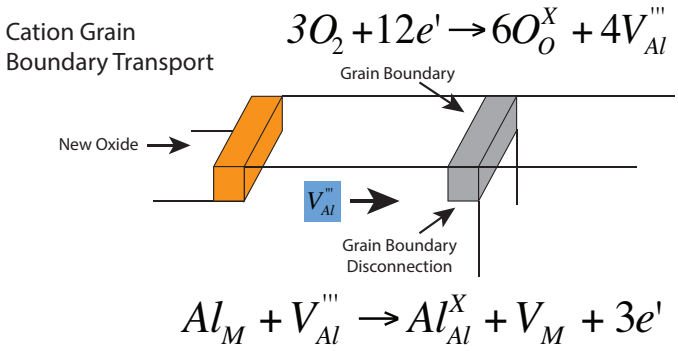

b)

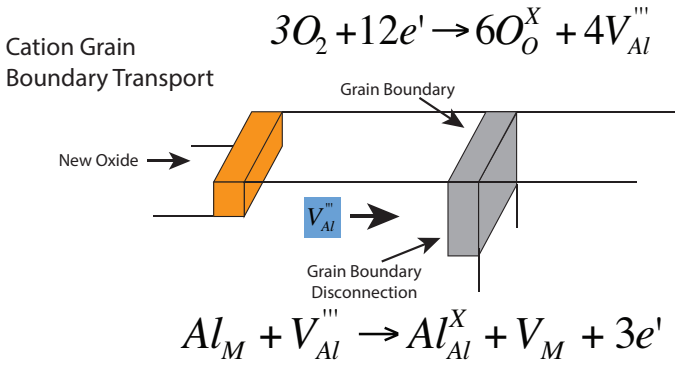

c)

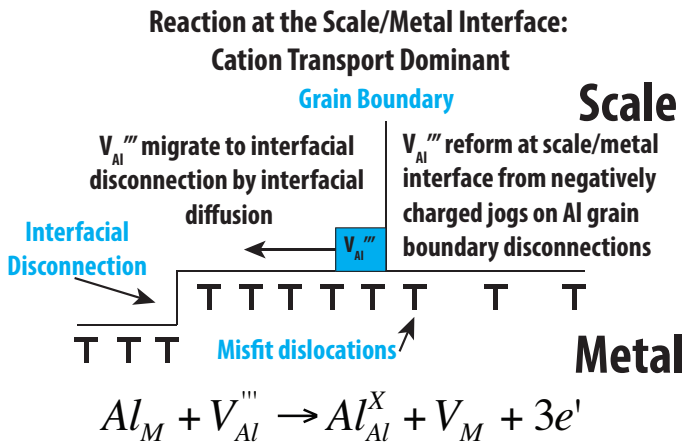

d)

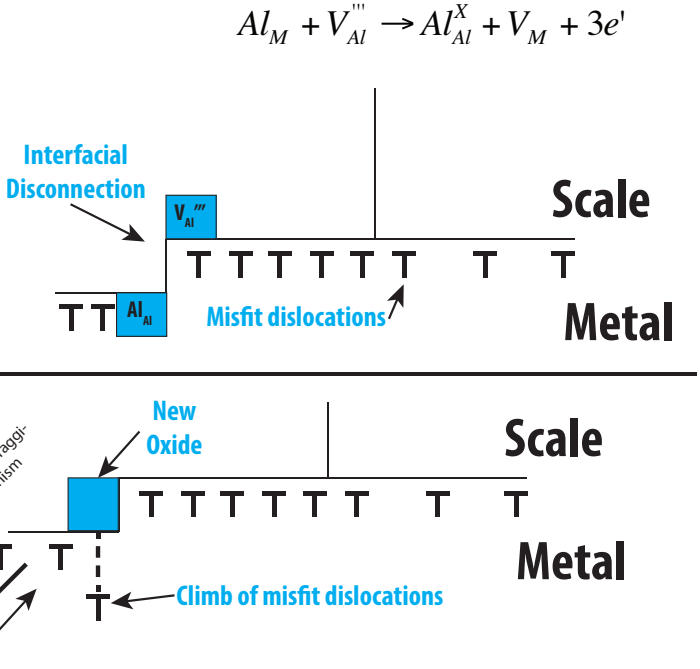

Figure 7

a)

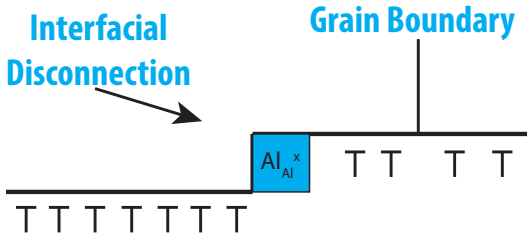

$$2Al_M \rightarrow 3V_O^{\bullet\bullet} + 2Al_{Al}^{x} + 2V_M + 6e'$$

b)

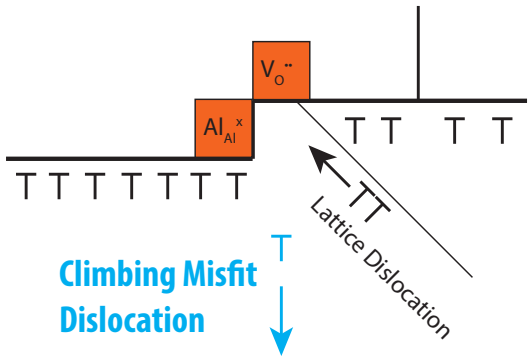

c)

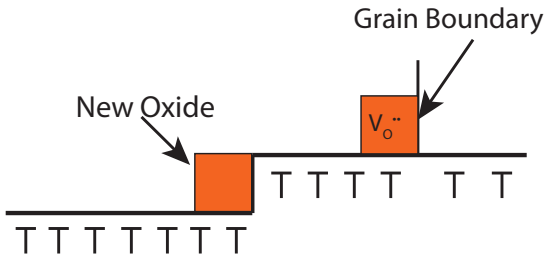

Oxygen vacancies are annihilated at grain boundary disconnections to form positively charged grain boundary jogs which migrate towards the scale/gas interface.

d)

$$O_2 + 2V_O^{\bullet\bullet} \rightarrow 2O_O^{X} + 4h^{\bullet}$$

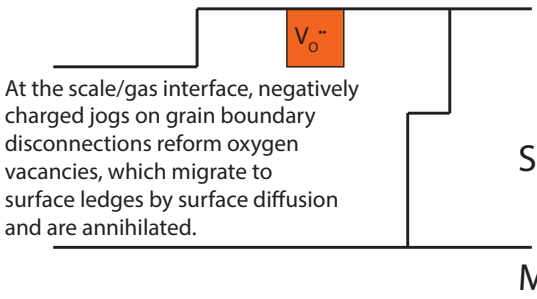

At the scale/gas interface, negatively charged jogs on grain boundary disconnections reform oxygen vacancies, which migrate to surface ledges by surface diffusion and are annihilated.

$$2Al_M \rightarrow 3V_O^{\bullet\bullet} + 2Al_{Al}^{x} + 2V_M + 6e'$$

Figure 8

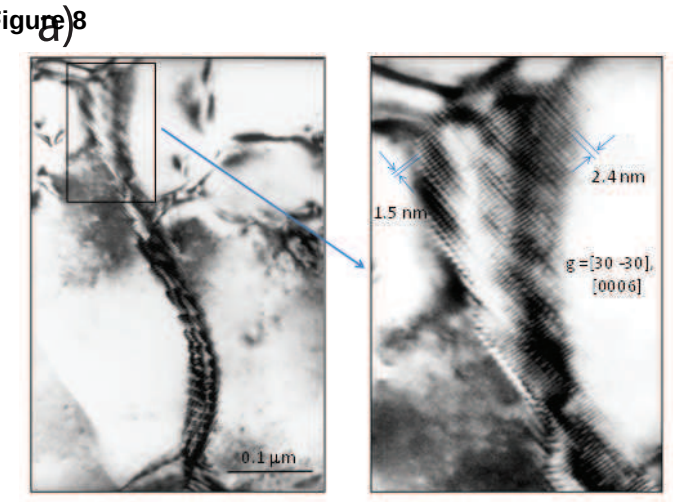
a)
0.1 µm
1.5 nm
2.4 nm
g = [30 -30], [0006]

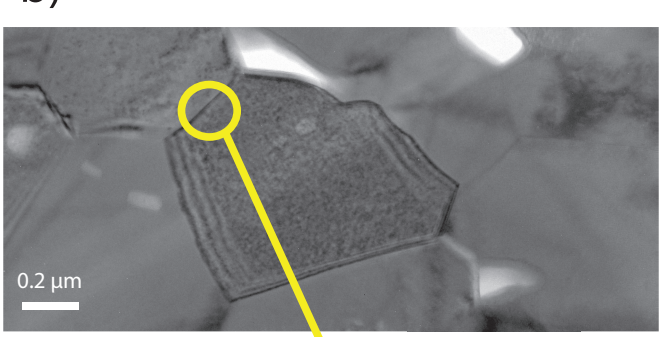
b)
0.2 µm

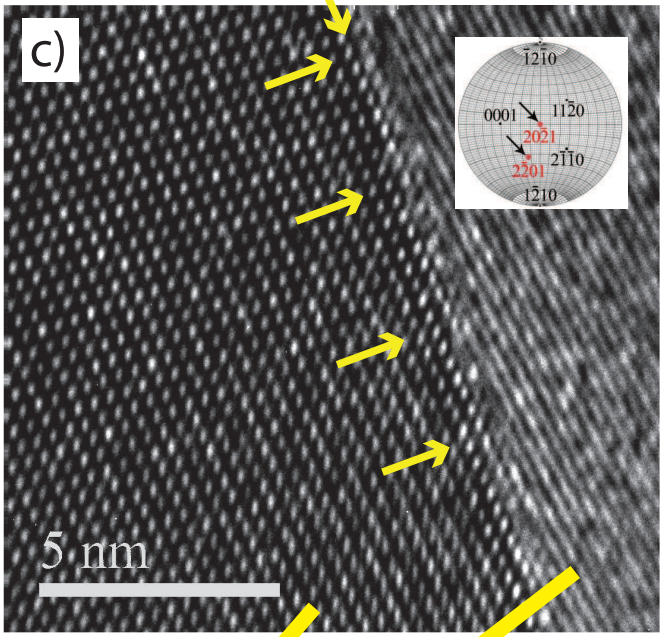
c)
5 nm

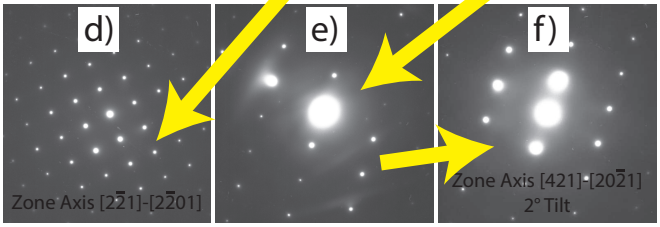
d)
e)
f)
Zone Axis [2$\bar{2}$1]-[2$\bar{2}$01]
Zone Axis [421]-[20$\bar{2}$1]
2° Tilt

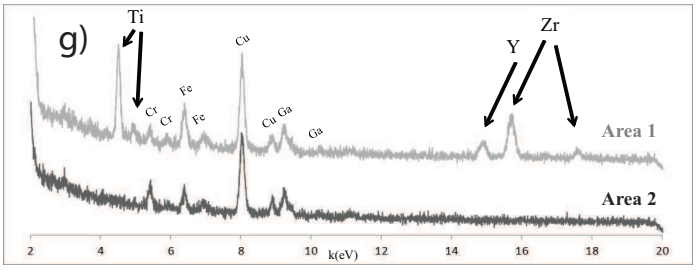
g)
Ti
Cr
Cr
Fe
Fe
Cu
Cu
Ga
Ga
Y
Zr
Area 1
Area 2
2
4
6
8
10
k(eV)
12
14
16
18
20

Figure 9

a)

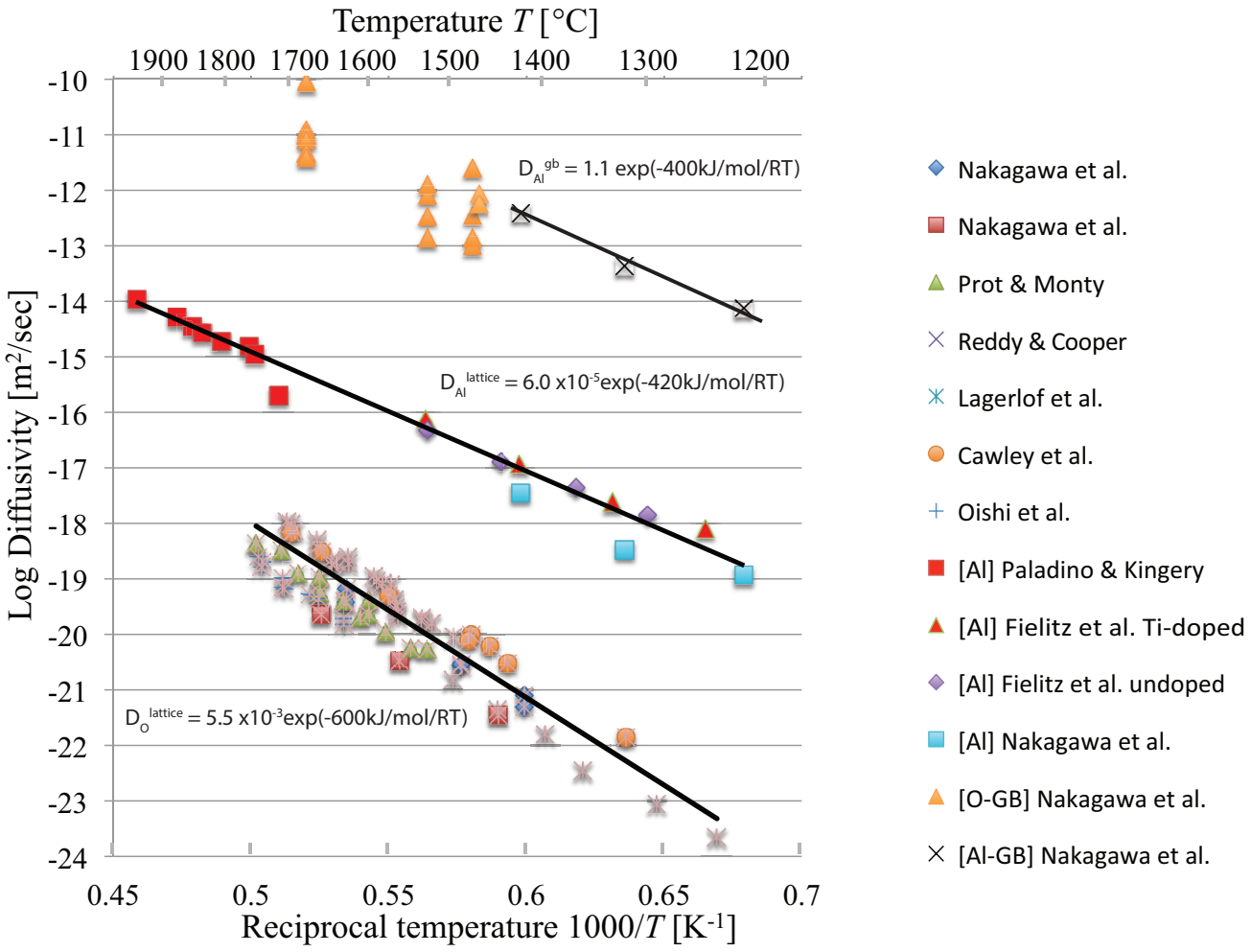

b)

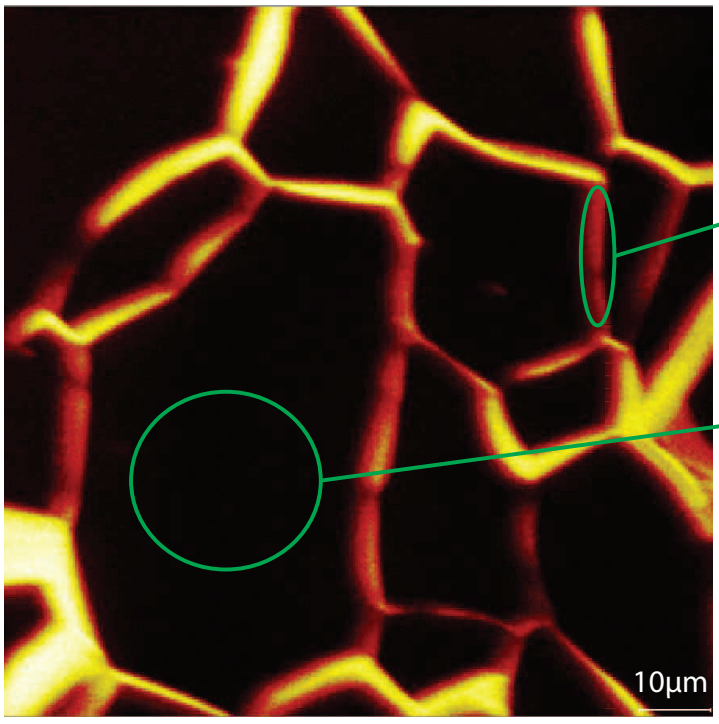

^{18}O grain boundary diffusion data: all grain boundaries are not equal!

^{18}O lattice diffusion data agress with previous literature

Field of view: 100µm x 100µm

Image is an average of the region between 0.5 and 2 µm below the surface